Particle Dark Matter constraints: the effect of Galactic uncertainties

To cite this article: Maria Benito *et al* JCAP02(2017)007

View the article online for updates and enhancements.

IOP Astronomy ebooks

Part of your publishing universe and your first choice for astronomy, astrophysics, solar physics and planetary science ebooks.

iopscience.org/books/aas

Particle Dark Matter constraints: the effect of Galactic uncertainties

Maria Benito,[a] **Nicolás Bernal,**[a,b] **Nassim Bozorgnia,**[c] **Francesca Calore**[c,d] **and Fabio Iocco**[a]

[a]ICTP South American Institute for Fundamental Research
Instituto de Física Teórica - Universidade Estadual Paulista (UNESP)
Rua Dr. Bento Teobaldo Ferraz 271, 01140-070 São Paulo, SP Brazil

[b]Centro de Investigaciones, Universidad Antonio Nariño
Cra 3 Este # 47A-15, Bogotá, Colombia

[c]GRAPPA Institute, Institute for Theoretical Physics Amsterdam
and Delta Institute for Theoretical Physics, University of Amsterdam,
Science Park 904, 1098 XH Amsterdam, The Netherlands

[d]LAPTh, CNRS, 9 Chemin de Bellevue, 74941 Annecy-le-Vieux, France

E-mail: mariabenitocst@gmail.com, nicolas.bernal@uan.edu.co,
n.bozorgnia@uva.nl, calore@lapth.cnrs.fr, fabio.iocco.astro@gmail.com

JCAP02(2017)007

Abstract. Collider, space, and Earth based experiments are now able to probe several extensions of the Standard Model of particle physics which provide viable dark matter candidates. Direct and indirect dark matter searches rely on inputs of astrophysical nature, such as the local dark matter density or the shape of the dark matter density profile in the target in object. The determination of these quantities is highly affected by astrophysical uncertainties. The latter, especially those for our own Galaxy, are ill-known, and often not fully accounted for when analyzing the phenomenology of particle physics models. In this paper we present a systematic, quantitative estimate of how astrophysical uncertainties on Galactic quantities (such as the local galactocentric distance, circular velocity, or the morphology of the stellar disk and bulge) propagate to the determination of the phenomenology of particle physics models, thus eventually affecting the determination of new physics parameters. We present results in the context of two specific extensions of the Standard Model (the Singlet Scalar and the Inert Doublet) that we adopt as case studies for their simplicity in illustrating the magnitude and impact of such uncertainties on the parameter space of the particle physics model itself. Our findings point toward very relevant effects of current Galactic uncertainties on the determination of particle physics parameters, and urge a systematic estimate of such uncertainties in more complex scenarios, in order to achieve constraints on the determination of new physics that realistically include all known uncertainties.

Contents

1 Introduction

Searches for the very nature of the elusive *dark* component of matter (DM) are experiencing a crucial moment in these very years: the enhanced sensitivity of direct and indirect searches, together with the latest data coming from collider experiments, allows to constrain the parameter space of several extensions of the Standard Model (SM) of particle physics, in some cases strongly challenging models which have been very popular in the last years. The multichannel searches for DM are seeing the dawn of a real precision era. The grandeur of this endeavor carries the burden of precision, and it becomes timely and mandatory to properly assess the entire budget of uncertainties that affect such an amazingly refined construction. It is very well known, and we also recall in the following in more detail, that the particle interpretation of the data coming from direct and indirect searches depends on quantities of astrophysical nature, such as the spatial distribution of DM in the target for indirect searches, and its phase space distribution in the solar neighborhood for direct ones. Strenuous efforts are ongoing from the side of the astrophysical community to assess these quantities, in a major endeavor involving astronomical observations of diverse nature. Yet, the determination of the quantities of interest are affected by often sizable uncertainties. This is also well known in the literature, where the entire extent of these uncertainties does not always propagate its way in the determination of new physics.

In this work, we aim at presenting a case study by systematically analyzing how the uncertainties on the DM structure in our Galaxy affect the determination of new physics. We will use two of the simplest possible extensions of the SM: the Singlet Scalar (SSDM) and the Inert Doublet (IDM) DM models. Those models have been chosen as ideal testbeds given the relatively simple dependence of their phenomenology on a limited set of parameters, which makes it easy to visualize the effects of astrophysical (and in this case especially, Galactic) uncertainties in the parameter space of the particle physics model itself. Our goal is to prompt the evidence for the relevance of the propagation of known, but too often overlooked,

unknowns of astrophysical nature directly into the determination of new physics. In order to do so, we first present the most recent results on the determination of the DM distribution in our Galaxy, and most relevantly its uncertainties. We then show the dependence of DM direct and indirect searches on the Galactic uncertainties, and specify how the constraints on the parameters of the IDM and SSDM models set by direct and indirect searches are affected by such uncertainties.[1]

The paper has the following structure. In section 2 we describe the setups of our analysis: datasets and techniques adopted for the determination of the DM density structure of the Milky Way (MW); the adopted benchmark limits for DM direct detection; and the probes chosen as indirect detection targets. In section 3 we describe our benchmark particle physics models: extensions of the SM which provide a well posed DM candidate, and have recently been claimed to be strongly constrained by existing data. In section 4 we present the finding of our analysis, and the impact of uncertainties on the Galactic baryonic morphology and parameters on the determination of new physics. In our conclusions, we summarize our key results and motivate how they prompt the extension of a similar complete analysis to more complex extensions of the SM.

2 Setups

2.1 Galactic dynamics

In order to determine the DM density profile of our own Galaxy, we adopt a well known dynamical method: objects in circular orbits around the Galactic center (GC) are used as tracers of the total gravitational potential, and the rotation curve (RC) thus obtained (in the plane of the disk) is compared to the circular velocity expected to be caused by the visible component of the MW alone. The mismatch between the two is accounted for by a non visible, *dark* component of matter, whose density distribution can be obtained by fitting an appropriately parametrized function to the total RC. This class of methods, often known as *global methods*, offers a series of advantages with respect to *local* ones, which permit to determine the DM distribution only in a small region around the location of the Sun, and a series of shortcomings. Both are carefully described in the recent review [1], and while addressing the reader to it and references therein for a complete overview, we highlight here the advantages and shortcomings of relevance to this specific analysis. We follow the recent analysis in [2], which respect to previous similar studies [3–5], offers the remarkable improvement to adopt a vast range of data-driven morphologies for the three visible components of the MW (stellar bulge, stellar disk(s), gaseous disk). As shown therein, the choice of stellar bulge/disk affects the shape of the DM profile beyond the statistical uncertainties associated to each one of the visible components, leading to the conclusion that our ignorance on the morphology of the MW hinders our determination of the DM profile more than the uncertainties associated to their normalization. Also, a quantitative estimate of the effect of the currently quoted uncertainties on the Galactic parameters (R_0, v_0) is offered, showing effects comparable with that of the Galactic morphology. This matter is certainly well known in principle, but again its actual magnitude is ill-known, and its effect on the determination of new physics is equally unaccounted for in most of the literature. Unfortunately, none of these uncertainties are easily treatable in a statistical way, and one

---

[1] We remark that the variability of the direct detection exclusion limits or indirect detection reconstruction contours presented in this work cannot be interpreted as 1 σ intervals.

runs the risk to underestimate the effect of cross-correlations between datasets, or to be affected by hidden biases in the choice of the null hypothesis. For this reason, we aim here only to offer an estimate of the effects *in the parameter space of particle physics models*, by varying different sources of uncertainty one at a time. Anticipating our results, we state here that our study motivates an effort from the community to treat all the uncertainties together in a self-consistent way, with the aim of adopting statistically valid methods to reduce the large astrophysical uncertainties now affecting new physics determination.

By combining together one by one all possible combinations of bulge, disk, and gas, we obtain a set of unique "baryonic morphologies", i.e. a catalogue of observationally-inferred morphologies, each one of them carrying a statistical uncertainty arising from the normalization of the density profile of each component, which is then propagated to the corresponding RC (generated by that specific configuration of visible matter) [2, 6]. For each baryonic morphology (throughout the paper we will refer to this simply as "morphology" for the sake of simplicity) and each set of Galactic parameters, separately, we add the RC due to DM to the one due to visible matter. The DM density profile is parameterised though a generalised NFW (gNFW) profile:

$$\rho_{\rm DM}(R) = \rho_0 \left(\frac{R_0}{R} \right)^\gamma \left(\frac{R_s + R_0}{R_s + R} \right)^{3-\gamma} , \tag{2.1}$$

where R_0 is the distance of the Sun from the GC, ρ_0 the DM "local" density (i.e. at the Solar position), R_s the so-called "scale radius" of the DM density profile, and γ the so-called "profile index" (the standard NFW profile having $\gamma=1$). We compare the resulting "total" (baryon + DM) RC to the latest compilation of observed RC data, presented in [6]. Following closely the methodology of [2], we scan the (ρ_0, γ) space, while keeping the scale radius R_s constant. We determine the goodness of fit of each point in the parameter space using the two-dimensional variable:

$$\chi^2 = \sum_{i=1}^N d_i^2 \equiv \sum_{i=1}^N \left[\frac{(y_i - y_{t,i})^2}{\sigma_{y,i}^2 + \sigma_{b,i}^2} + \frac{(x_i - x_{t,i})^2}{\sigma_{x,i}^2} \right] , \tag{2.2}$$

where we have introduced the reduced variables $x = R/R_0$ and $y = w/w_0 - 1$; $(x_i \pm \sigma_{x,i}, y_i \pm \sigma_{y,i})$ are the RC measurements, $\sigma_{b,i}$ is the uncertainty of the individual baryonic model evaluated at x_i and $(x_{t,i}, y_{t,i})$ are the points that minimize d_i along the curve $y_t(x) = w_t(R = xR_0)/w_0 - 1$. The variable $w(R) = v_c(r)/R$ is the angular velocity at the galactocentric distance R (with $w_0=w(R_0)$), and it is used as an independent variable as the uncertainties on R and w are uncorrelated (see [6] and references therein). The sum runs over all the N objects in the compilation at $R > R_{\rm cut} = 2.5$ kpc in order to exclude the innermost regions of the Galaxy where axisymmetry breaks down and some tracers may present non-circular orbits. The function in eq. (2.2) has been shown to have a χ^2 distribution for the case at hand in [6], and offers the advantage of an unbinned analysis which properly takes into account the statistical uncertainties of the observed RC dataset (in both dimensions), and that of the baryonic RC, propagated from the normalization of the stellar bulge and disk (respectively from microlensing optical depth in the direction of the bulge and local stellar surface density, see [2, 4] for methodology, and references therein). The "best fit" point is obtained by picking the point in (ρ_0, γ) space that minimizes the two dimensional χ^2 described above, while we have kept the scale radius constant at the value $R_s=20$ kpc. We note that also the variation of R_s is expected to have some impact. Although we have tested that the choice of a fixed

R_s value does not affect significantly our conclusions, a full analysis of the effect of the R_s variation is beyond the scope of the present paper and we postpone it to a future work.[2]

In order to probe the effect of different sources of ignorance, we test the following uncertainties one at a time:

- Statistical uncertainties;

- Uncertainties on Galactic parameters, (R_0, v_0);

- Uncertainties on the morphology of the visible, i.e. baryonic, component of the Galaxy.

The numerical values adopted, the results obtained, as well as the reference for the morphologies that comply with the above conditions are presented schematically in table 1, and we summarize here the criteria behind the choices adopted, according to the above rationale:

- *Standard Galactic parameters.* The "standard" Galactic parameter values are $(R_0, v_0) = (8\text{kpc}, 230\text{km/s})$. When these values are adopted, the peak speed of the Maxwellian velocity distribution of DM particles is taken to be equal to the local circular speed, $v_{\text{peak}} = v_0 = 230$ km/s.[3]

- *Reference morphology.* The "representative" baryonic morphology is [8–11]; referred to as "*BjX* " in table 1.

- *Galactic parameters variation.* The extreme values for the Galactic parameters are chosen to vary between R_0=[7.5–8.5] kpc and v_0=[180–312] km/s, for our representative morphology *BjX*. The local circular speed can range from (200 ± 20) km/s to (279 ± 33) km/s [12]. Hence, we take $v_0 = 180$ km/s and 312 km/s as lower and higher estimates, respectively. When these values are adopted for v_0, we take $v_{\text{peak}} = 250$ km/s, regardless of v_0.[3]

- *Morphology variation.* The extreme baryonic morphologies are chosen to be those that require the maximum/minimum values of γ, ρ_0, in order to visualize the maximum impact on both direct and indirect detection as we will see in the following sections.

With reference to the nomenclature in table 1, we find that (for assigned, standard Galactic parameters) the baryonic morphologies that maximize/minimize

- the index γ are respectively "*FkX*" and "*DiX*";

- the local DM density ρ_0 are respectively "*CjX*" and "*FiX*".

In figure 1 we display the rotation curves corresponding to the baryonic morphologies described above, assuming fixed Galactic parameters (R_0, v_0)=(8 kpc, 230 km/s). Statistical

---

[2]We checked that by varying its value by a factor 2 we observe a maximal variation in the local DM density of ≲5%, and on the $\mathcal{J}$-factor (see section 2.3 for the definition of $\mathcal{J}$-factor) of ≲10% for the region of interest of the GC GeV excess. As it will be seen, this is well below the effects of the variation of baryonic morphology or Galactic parameters.

[3]This choice for the peak speed of the Maxwellian velocity distribution falls in the range of [223–289] km/s suggested by high resolution hydrodynamic simulations [7] (see also section 2.2). We have checked that varying v_{peak} does not make a visible difference in the direct detection limits in the parameter space of the SSDM and IDM models, and its effect is much smaller than the effect of variation of other Galactic parameters.

Morphology	R_0 (kpc)	v_0 (km/s)	M_* ($\times 10^{10} M_\odot$)	γ	ρ_0 (GeV/cm^3)	χ^2/dof	Reference
BjX	8	230	2.4 ± 0.5	$1.11^{+0.04}_{-0.03}$	0.466 ± 0.010	1.22	[8–11]
BjX	7.5	312	1.52 ± 0.19	$0.633^{+0.019}_{-0.020}$	1.762 ± 0.017	1.35	[8–11]
BjX	8.5	180	2.4 ± 0.5	2.02 ± 0.07	0.055 ± 0.004	0.90	[8–11]
FkX	8	230	2.0 ± 0.4	$1.38^{+0.03}_{-0.02}$	$0.427^{+0.007}_{-0.008}$	1.05	[10, 11, 24, 25]
DiX	8	230	3.0 ± 0.6	$0.43^{+0.07}_{-0.06}$	0.405 ± 0.011	0.99	[10, 11, 26, 27]
CjX	8	230	2.5 ± 0.6	1.03 ± 0.04	$0.471^{+0.010}_{-0.011}$	1.13	[9–11, 28]
FiX	8	230	2.6 ± 0.4	0.82 ± 0.05	0.387 ± 0.010	1.16	[10, 11, 24, 27]

Table 1. We adopt a gNFW density profile with $R_s = 20$ kpc. From left to right we report the nomenclature adopted for each morphology, the values of Galactic parameters (R_0, v_0), the baryonic mass in the Galaxy for that specific baryonic morphology, the best-fit values of index γ and ρ_0 according to the procedure described in the text, the value of χ^2 per degree of freedom, and the references for the three-dimensional morphology shape. Quoted uncertainties are 1 σ (68% confidence level) here and elsewhere unless otherwise stated. The criteria that led to the choice of these morphologies are explained in the text.

uncertainties associated to the displayed central values are not shown, but they are taken into account for the fitting procedure as described above. We also display our compilation of data for the observed RC and their 1σ uncertainties, as originally presented in [6]. In order to normalize the data to different values of the Galactic parameters, we have used the publicly available tool *galkin*, [13]. In table 1 we report the results of the fitting procedure described and the parameters of the selected morphologies.

When varying Galactic parameters, we obtain the total mass of the MW within 50 kpc to be in the range M(< 50 kpc) $= (0.7 - 22.5) \times 10^{11}$ M$_\odot$. The lower limit is in agreement with previous determinations [14–18], while the larger MW masses we obtain can not be directly compared, as the the adopted Galactic Parameters are different than ours. When varying baryonic morphology, the minimum/maximum values obtain are M(< 50 kpc) $= 4.6^{+0.7}_{-0.6} \times 10^{11}$ M$_\odot$ and M(< 50 kpc) $= 7.1^{+0.19}_{-0.18} \times 10^{11}$ M$_\odot$. The former value for the variation of morphology is in good agreement with mass estimate from kinematics of globular clusters, satellite galaxies and halo stars [14, 15, 17, 19]. There is, however, a discrepancy at the 1σ level with the independent determination in [18], that used the Sagittarius stream, and is slightly higher than the other cited determinations. All our results are in agreement at the 1σ level with the recent estimate of the dynamical mass [20] within the region of the Galactic bulge, as in the analysis presented in [21].

In figure 2, we show the DM density profiles corresponding to the selected morphologies in table 1. When varying the morphology, almost all DM profiles are in agreement with recent findings for MW-like galaxies in hydrodynamical simulations [22, 23]. The upper panel displays the DM density as a function of the distance from the GC, while in the lower panel the relative error with respect to the reference model is shown. As a reference we also depict the traditionally adopted NFW profile, corresponding to a gNFW with parameters $\gamma = 1$, $\rho_0 = 0.4$ GeV/cm^3.

2.2 Direct detection

The aim of direct detection experiments is to measure the small recoil energy of a nucleus in an underground detector after the collision with a WIMP arriving from the DM halo of the MW.
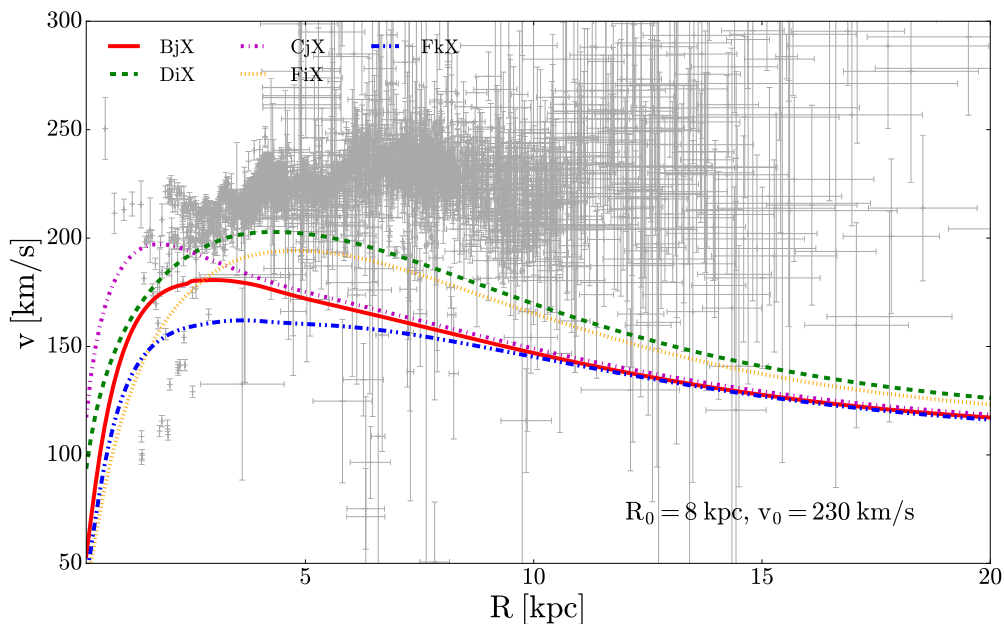
Figure 1. RC produced by the benchmark baryonic morphologies (colored curves), reported in table 1 and described in the text. RC data points and their 1σ errors shown in gray are from the compilation presented in [6].
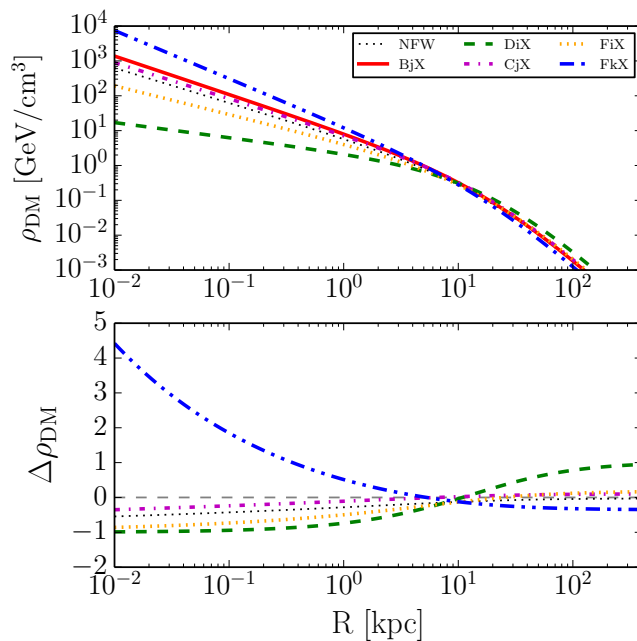

Figure 2. The DM density, $\rho_{\rm DM}$, as a function of radial distance from the GC, R, for a standard NFW profile (black dotted line), and all baryonic morphologies in table 1 with standard Galactic parameters, as described in the text. The bottom panel refers to the relative error of $\rho_{\rm DM}$ with respect to the reference morphology BjX. The dashed gray line in the bottom panel corresponds to a perfect match between the morphology considered and the BjX.

The current status of direct detection searches is ambiguous with a few experiments reporting hints for a DM signal [29–32], while all other experiments report null-results. Currently the LUX (Large Underground Xenon) experiment [33] places the strongest exclusion limit in the plane of spin-independent DM-nucleon cross section and WIMP mass for large DM masses, while the PandaX-II (Particle and Astrophysical Xenon Detector) experiment [34] has recently reported competitive null results. In this paper we focus on the impact of astrophysical uncertainties on the LUX exclusion limit in the parameter space of specific particle physics models. However, we note that the variation of the exclusion limits set by other direct detection experiments due to astrophysical uncertainties would be similar to those discussed for LUX.

For a DM particle scattering elastically off a nucleus with atomic mass number A, the differential event rate (per unit energy, per unit detector mass, per unit time) in direct detection experiments for the case of spin-independent scattering can be written as,

$$\frac{dR}{dE_R} = \frac{\rho_0 \, A^2 \, \sigma_{\rm SI}}{2 \, m_{\rm DM} \, \mu_p^2} \, F^2(E_R) \, \eta(v_{\rm min}, t), \tag{2.3}$$

where E_R is the nuclear recoil energy, ρ_0 is the local DM density, $m_{\rm DM}$ is the DM mass, μ_p is the reduced mass of the DM-nucleon system, $\sigma_{\rm SI}$ is the spin-independent DM-nucleon scattering cross section, and $F(E_R)$ is a form factor. $v_{\rm min} = \sqrt{m_A E_R/(2\mu_A^2)}$ is the minimum speed needed for the DM particle to deposit a recoil energy E_R in the detector. Here m_A is the mass of the nucleus, and μ_A is the DM-nucleus reduced mass. The halo integral, $\eta(v_{\rm min}, t)$, which together with the local DM density encompasses the astrophysics dependence of the recoil rate, is defined as,

$$\eta(v_{\rm min}, t) \equiv \int_{v > v_{\rm mim}} d^3 v \frac{f_{\rm det}(\mathbf{v}, t)}{v}, \tag{2.4}$$

where $f_{\rm det}(\mathbf{v}, t)$ is the local DM velocity distribution in the detector rest frame.

Eq. (2.3) can be written as,

$$\frac{dR}{dE_R} = C_{\rm PP} \, F^2(E_R) \, \rho_0 \, \eta(v_{\rm min}, t), \tag{2.5}$$

where the coefficient $C_{\rm PP} = A^2 \sigma_{\rm SI}/(2 \, m_{\rm DM} \, \mu_p^2)$ contains the particle physics dependence of the event rate, while $\rho_0 \, \eta(v_{\rm min}, t)$ contains the astrophysics dependence.

In the analysis of direct detection data, usually the Standard Halo Model (SHM) is adopted. In the SHM, the DM halo is spherical and isothermal, and the local DM velocity distribution is an isotropic Maxwell-Boltzmann distribution with a peak speed, $v_{\rm peak}$ equal to the local circular speed, v_0.

The results of state-of-the-art high resolution cosmological simulations which include both DM and baryons indicate that a Maxwellian distribution with a best fit peak speed in the range of 223–289 km/s fits well the local velocity distribution of simulated MW-like haloes [7]. Based on the results of ref. [7], for the analysis of direct detection data in this work we adopt a Maxwellian velocity distribution truncated at the Galactic escape speed, and with a peak speed in the range of $[223 - 289]$ km/s, independent from the local circular speed. For the local circular speed, we adopt $v_0 = 180$ km/s and 312 km/s as high and low estimates. For the peculiar velocity of the Sun with respect to the Local Standard of Rest we assume $(11.10, 12.24, 7.25)$ km/s [35] in Galactic coordinates. We adopt the median value of the local Galactic escape speed reported by the RAVE survey, $v_{\rm esc} = 533$ km/s [36].
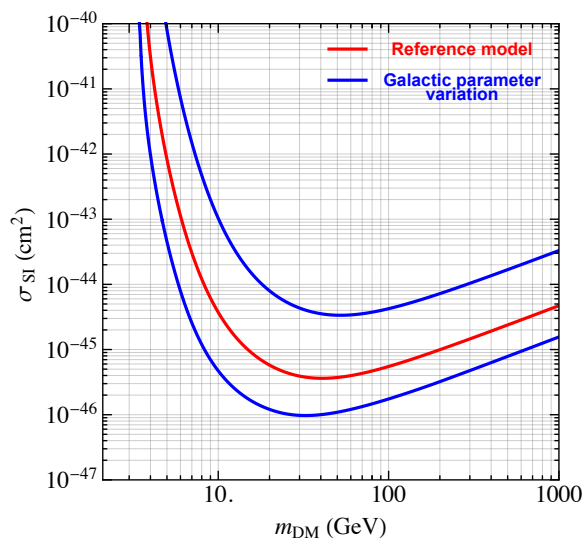
Figure 3. LUX exclusion limit at 90% CL in the spin-independent DM-nucleon cross section and DM mass plane for the reference choice of Galactic parameters and local DM density (red curve) given in the first row of table 1, and two variations of Galactic parameters and local DM density (blue curves) given in the second and third rows of table 1, see text in section 2.1 for a complete description.

Recently, the LUX experiment has reported the results of 332 live days of data, with no evidence of a DM signal [33]. Since the exposure and detector response information is not publicly available for each event in the recent LUX data, we perform an analysis of the 2015 LUX results [37] instead. In ref. [37], the LUX collaboration presented an improved analysis of their 2013 data for an exposure of 1.4×10^4 kg days. To set an exclusion limit using the LUX data, we employ the maximum gap method [38], since we cannot reproduce the likelihood analysis performed by the LUX collaboration with the available information. We consider the events which fall below the mean of the nuclear recoil band (red solid curve in figure 2 of [37]) as signal events, and assume an additional acceptance of 0.5. As seen from figure 2 of [37], one event makes the cut. We take the detection efficiency from figure 1 of [37], and set it equal to zero below the recoil energy of $E_R = 1.1$ keV, following the collaboration. Since we are only interested in events at < 18 cm radius, we multiply the efficiency by $(18/20)^2$. To find the relation between E_R and the primary scintillation signal S1, we find the value of S1 at the intersection of each recoil energy contour and the mean nuclear recoil curve from figure 2 of [37]. Assuming a Maxwellian velocity distribution with the same parameters as in [37], we can find an exclusion limit at 90% CL which agrees well with the limit set by the LUX collaboration.

In figure 3, we show the LUX exclusion limit in the $m_{\rm DM} - \sigma_{\rm SI}$ plane for the standard choice of Galactic parameters (R_0, v_0) and the local DM density ρ_0 for our reference morphology given in the first row of table 1 ("reference model" in figure legend), as well as for two representative variations of Galactic parameters and ρ_0 given in the second and third rows of table 1. The largest variation of the exclusion limit with respect to the reference limit is due to the variation in the local DM density. Notice that in the exclusion limits shown in figure 3, we take $v_{\rm peak} = v_0$, while in the figures of section 4 where we vary the Galactic parameters, we adopt a peak speed value independent of the local circular speed.

2.3 Indirect detection

Indirect detection aims at detecting the flux of final stable particles produced by DM annihilation or decay. Among those, gamma rays are considered the golden channel for the identification of a possible DM signal since they preserve the spectral and spatial information of the signal itself. In the present work, we focus on the gamma-ray flux from DM annihilation for a twofold reason: first, we work with gamma rays since the expected flux is directly expressed in terms of the DM density distribution. For charged cosmic rays, instead, the expected flux at Earth is obtained after propagating the produced particles in the interstellar medium and thus the dependence of the propagated flux on the DM density is less trivial.[4] Secondly, the choice of the annihilation process — instead of the decay one — is motivated by the fact that the predicted flux is more affected by the astrophysical uncertainties on the DM density, since it depends on the DM density squared. We stress that our aim is to give concrete — and intuitive — examples of the effect of the astrophysical uncertainties for DM phenomenology.

Typically, the gamma-ray flux from DM particles annihilation or decay can be factorized in terms of a particle physics term, $\Phi_{\rm PP}$, which contains the information of the underlying particle physics theory of DM, and an astrophysical term, $\mathcal{J}$, which instead encodes the information about the geometrical distribution of DM in space. The DM expected flux writes as:

$$\Phi_{\rm DM}(E) = \Phi_{\rm PP}(E)\,\mathcal{J}\,. \tag{2.6}$$

In this section, we remain agnostic about the particle physics sector, while we are interested in quantifying the uncertainty affecting the $\mathcal{J}$-factor in light of the analysis performed in section 2.1. The $\mathcal{J}$-factor is defined as the integral along the line-of-sight of the DM density, $\rho_{\rm DM}$, in case of DM decay, or of the DM density squared, $\rho_{\rm DM}^2$, in case of DM annihilation. While the uncertainty of $\rho_{\rm DM}$ translates linearly in the uncertainty on $\mathcal{J}_{\rm decay}$, the $\mathcal{J}_{\rm annih}$ is more sensitive to the uncertainty on $\rho_{\rm DM}$ given the squared dependence. In the case of DM annihilation:

$$\mathcal{J}_{\rm annih} = \int_{\rm l.o.s} \rho_{\rm DM}^2(R(l,\psi))dl, \tag{2.7}$$

where ψ is the opening angle between the line of sight l and the direction towards the GC. The radial distance from the GC is $R^2 = R_0^2 + l^2 - 2\,l\,R_0\,\cos(\psi)$.

In figure 4 we show the uncertainty on the DM annihilation $\mathcal{J}$-factor (bottom panel) for different morphologies as in figure 2 (cf. table 1). In the upper panel, we show the $\mathcal{J}$-factor as a function of the angle ψ, comparing a standard NFW profile with our reference baryonic morphology and other morphology configurations, cf. table 1. In the inner region, i.e. within few degrees, the astrophysical uncertainty on the $\mathcal{J}$-factor is $\gtrsim \mathcal{O}(10)$.

Accounting for the astrophysical uncertainty on the predicted DM flux is crucial when comparing results from different targets. For example, a positive signal might be seen in a gamma-ray target and interpreted in terms of DM annihilation. The preferred particle physics parameter space, typically the average velocity annihilation cross section $\langle\sigma v\rangle$ vs DM mass $m_{\rm DM}$, depends on the $\mathcal{J}$-factor assumed for the target considered. On the other hand, null results from other targets impose upper limits on the allowed ($\langle\sigma v\rangle$, $m_{\rm DM}$) parameter space. It might occur that the constraints are in tension with the signal. However, such a tension relies on the assumed $\mathcal{J}$-factor and, thus, the uncertainty on the $\mathcal{J}$-factor must be

---

[4]We note however that the "source term" of charged particles produced by DM depends directly on the DM density and thus is affected by the same uncertainties that we discuss explicitly for gamma rays.

fully accounted for before claiming a strong tension. This is what happened for example in the case of the GC GeV excess (see e.g. [39, 40]), an anomalous emission of gamma rays coming from the inner region of the Galaxy. Various interpretation of this excess have been put forward, from astrophysical processes (e.g. [41–45]) to DM annihilation (e.g. [46, 47]). Although there is strong support for the GeV excess to arise from a population of faint, unresolved point sources, a DM interpretation has not been yet robustly excluded. For the illustrative purpose of the present paper, we assume that the GeV excess can be interpreted as due to DM particle annihilation in the halo of the MW. This interpretation started also to be challenged by the latest constraints from dwarf spheroidal galaxies (dSphs) [48].

Here we demonstrate that such a tension can be alleviated (or worsened) by the unavoidable uncertainty on the $\mathcal{J}$-factor of the MW — we do not discuss here the uncertainties on the dSphs $\mathcal{J}$-factor related to the choice of the dSphs DM profile (see e.g. [49] for a discussion).[5]

In figure 5, we show the latest dSphs limits [48] and the region preferred by the GC GeV excess for DM annihilating into a pair of b-quarks [46], for our reference morphology BjX with standard Galactic parameters ("reference model" in figure legend), and for the variation of Galactic parameters, as given in the second and third rows of table 1. For the sake of clarity we show only the 1 and 2σ contours rescaled to the morphology of interest from the contours in ref. [46]. The rescaling of the original contours (in figure 5 as well as in all other figures showing the GeV excess rescaled contours) is made by imposing that the GeV excess flux measured at $2\,\mathrm{GeV}$ and $5°$ away from the GC is conserved, in analogy to what done in ref. [46]. Indeed, at $5°$ away from the GC the GeV excess intensity has been shown to be almost independent on the assumption on the gNFW slope used in the data analysis.[6] Therefore, the rescaling of the contours only involves $\mathcal{J}(\psi = 5°)$, and not the integral over the full region-of-interest. The variation of the contours in $\langle \sigma v \rangle$ due to the uncertainty on Galactic parameters (R_0, v_0) can be larger than a factor of two in both directions. We emphasise that also constraints on DM from the annihilation in the MW halo or the GC region would be affected by an analogous uncertainty.

3 Particle physics benchmarks

We now apply the setup shown until now to some benchmark DM particle models, in order to show how the astrophysical uncertainties affect the determination of the physical parameters of the specific models at hand, in the context of DM direct and indirect detection. We concentrate on two minimal extensions of the SM, the SSDM and the IDM, as they are arguably among the most minimal models for which it is easy to quantify and visualize in a clear way the effects described above. We do expect that our results will prompt a generalization to more complex scenarios in which the effects are not so trivially discernible from effects due to the interplay of numerous model parameters. In this section we present the general framework of these two simple models and depict the state-of-the-art constraints

---

[5]We note that the dSphs limits do not depend on the choice of the Sun's position, R_0. In fact astronomical distance measurements, used in the $\mathcal{J}$-factor determination of the dSphs, are derived directly in heliocentric coordinates and therefore do not depend on the position of the Sun in the Galactic reference frame, see for example [50].

[6]We note that considering the full angular profile of the GeV excess can set a constraint on the slope, γ, of the DM density profile. However, we do not want to combine different constraints on the morphology of the DM MW halo, but only study the impact of uncertainties coming from the fit to RC. We therefore refer to an observable of the excess which is independent on γ.
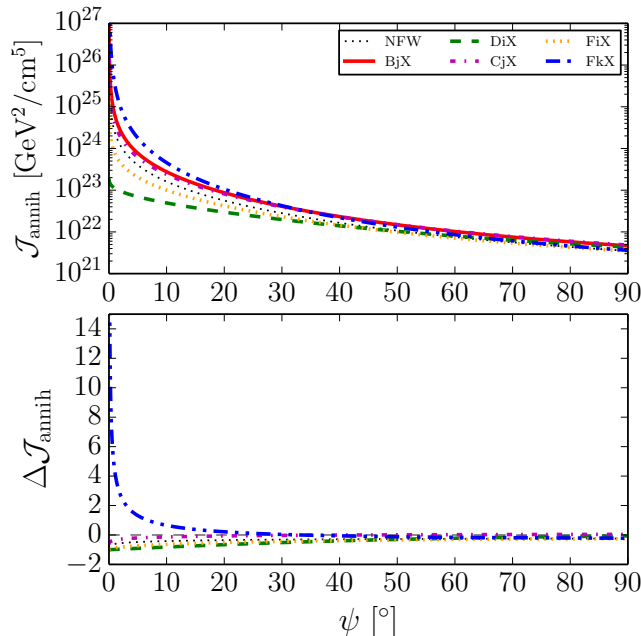
Figure 4. The DM annihilation $\mathcal{J}$-factor as a function of the angle ψ between the line-of-sight and the GC for the same DM profiles in table 1 and figure 2 (same colors). The bottom panel refers to the relative error of the $\mathcal{J}$-factor with respect to the reference morphology *BjX*. The dotted line corresponds to the traditional NFW profile. The dashed gray line in the bottom panels corresponds to a perfect match between the morphology considered and *BjX*.

on the model parameter space. The discussion of the impact of astrophysical uncertainties will be the focus of section 4.

3.1 Singlet Scalar Model

The SSDM [51, 52] is one of the minimal extensions of the SM that can provide a viable DM particle candidate. In addition to the SM, this model contains a real scalar S, singlet under the SM gauge group, but odd under a $\mathbb{Z}_2$ symmetry in order to guarantee its stability. The most general renormalizable scalar potential is given by

$$V = \mu_H^2 \, |H|^2 + \lambda_H \, |H|^4 + \mu_S^2 \, S^2 + \lambda_S \, S^4 + \lambda_{HS} \, |H|^2 \, S^2 \,, \tag{3.1}$$

where H is the SM Higgs doublet. It is required that the Higgs gets a non-vanishing vacuum expectation value, $v_H = 246 \, \text{GeV}$, while the singlet does not, $\langle S \rangle = 0$. At tree level, the singlet mass is $m_S^2 = 2 \, \mu_S^2 + \lambda_{HS} \, v_H^2$. The phenomenology of this model is completely determined by three parameters: the DM mass m_S, the Higgs portal coupling λ_{HS} and the quartic coupling λ_S. Note however that λ_S plays a minor role in vanilla WIMP DM phenomenology,[7] and thus hereafter we will focus only on the parameters m_S and λ_{HS}. These two parameters are the ones that determine the strength of both the direct and the indirect detection signals.

There has been a large amount of research on the SSDM, most of it focused on the WIMP scenario, where the singlet S mixes relatively strongly with the Higgs and undergoes

---

[7]Whereas λ_S has a crucial role in DM phenomenology, in scenarios where DM is a SIMP, with sizable self-interactions [53].
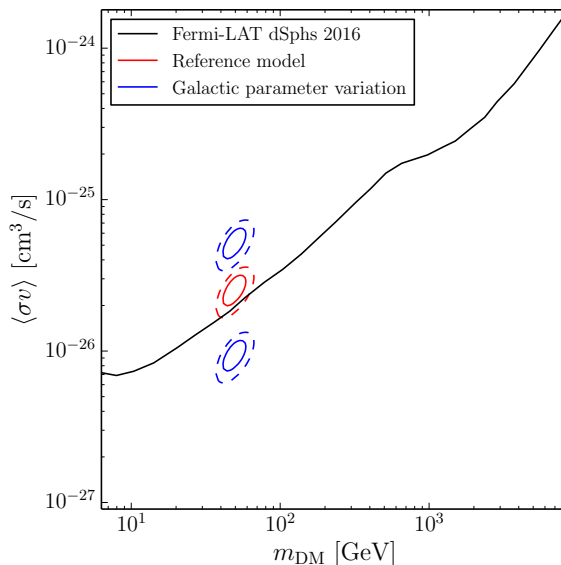
Figure 5. Upper limit on DM annihilation cross section (into $\bar{b}b$), $\langle \sigma v \rangle$, vs DM mass, $m_{\rm DM}$, from the analysis of gamma rays from dwarf spheroidal galaxies [48] (black line). Best fit contours at 2σ of the GeV excess as due to DM annihilation in b-quark pairs for the gNFW parameters preferred by our reference morphology *BjX* (red contours) with standard Galactic parameters, and the same morphology by varying Galactic parameters (blue countours), as given in the second and third rows of table 1, see text in section 2.1 for a complete description. This setup is the same as used for the variations in figure 3.

a thermal freeze-out. This scenario has been highly constrained by collider searches [54–60], DM direct detection [61–64] and indirect detection [65–71].

We show the current constraints in figure 6. In both panels, the black thick line corresponds to the points that generate a DM relic abundance in agreement with the measurements by Planck [72], and the gray region below the line is excluded because it produces a too large DM abundance, thus overclosing the Universe. The hatched light blue region in the upper left corner is forbidden by current constraints on the strength of the Higgs portal. Indeed, for $m_S < m_{h^0}/2 \sim 62$ GeV, the Higgs can decay into a pair of DM particles, thus the current limits on the invisible Higgs branching ratio ($\rm BR_{inv} \lesssim 20\%$ [73]) and the Higgs total decay width ($\Gamma_{h^0}^{\rm tot} \lesssim 22$ MeV [74]) constrain the Higgs coupling with the dark sector, λ_{HS}.

In the left panel of figure 6, we display the exclusion limit on the spin-independent elastic WIMP-nucleon cross section at 90% CL from the 2015 LUX results [37], which is translated into the dark red region in the top part of the figure. We plot here the limit derived from the red curve in figure 3 described in section 2.2. We recall that this limit has been derived assuming the parameters in the first row of table 1, i.e. a Maxwellian velocity distribution with $v_{\rm peak} = v_0 = 230$ km/s, $v_{\rm esc} = 533$ km/s, and $\rho_0 = 0.466$ GeV/cm^3. In the right panel, we show instead the current limits from the analysis of dwarf spheroidal galaxies (dSphs) with *Fermi*-LAT [48]. The region in blue represents the parameter space favoured by the interpretation of the GC excess (at 2σ), and corresponds to the red contour in figure 5, as described in section 2.3.

From figure 3, we see that the LUX limit strongly depends on the astrophysical uncertainties on the Galactic parameters, and especially on the uncertainty in the local DM density. Therefore, the available parameter space of the SSDM will depend on the actual
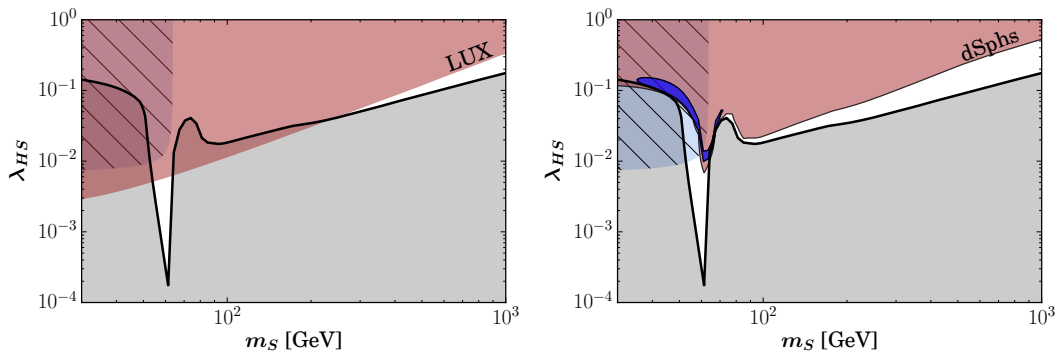
Figure 6. *Singlet Scalar Model.* In both panels, the black line corresponds to the points that generate a DM relic abundance in accordance to the measurements by Planck [72]; the lower gray region over-closes the Universe. The upper left region (hatched light blue) is ruled out by the invisible decay of the Higgs [73, 74]. The upper dark red region in the left panel corresponds to the LUX exclusion limit on the spin-independent elastic WIMP-nucleon cross section at 90% CL for the choice of parameters in the first row of table 1, while the one in the right panel is derived from the limits on the averaged velocity annihilation cross section from the combined analysis of dwarf spheroidal galaxies in the MW [48]. The parameter space favoured by the GeV excess data [46] (at 2σ) is depicted by the blue region in the right panel.

configuration of Galactic parameters. On the other hand, in the case of indirect searches, we do not explore uncertainties on the limits imposed by dSphs, but we investigate how the region favoured by the DM interpretation of the GeV excess will move because of Galactic uncertainties, as already shown in figure 5. We will show the response of the constraints to astrophysical uncertainties, and its implications in section 4.

3.2 Inert Doublet Model

The IDM [75] is another minimal extension of the SM that contains a second complex scalar doublet. The model contains an exact $\mathbb{Z}_2$ symmetry under which all SM particles –including one of the scalar doublets– are even, and the second scalar doublet is odd. Since this discrete symmetry prevents mixing between the scalars, one of the doublets (H) is identified with the SM Higgs doublet. The second doublet (Φ), odd under the $\mathbb{Z}_2$ parity, is inert in the sense that it does not couple to the SM particles. The most general renormalizable scalar potential of the IDM is given by

$$V = \mu_1^2 |H|^2 + \mu_2^2 |\Phi|^2 + \lambda_1 |H|^4 + \lambda_2 |\Phi|^4 + \lambda_3 |H|^2 |\Phi|^2 + \lambda_4 |H^\dagger \Phi|^2 + \frac{\lambda_5}{2} \left[(H^\dagger \Phi)^2 + \text{h.c.} \right]. \quad (3.2)$$

In the general case, the λ_i are complex parameters. Although considering this possibility can have interesting consequences for CP-violation and electroweak baryogenesis [76–78], in this work we limit ourselves to the case of real values. Upon electroweak symmetry breaking, the two doublets can be expanded in components as

$$H = \begin{pmatrix} 0 \\ \frac{1}{\sqrt{2}} \left(v_H + h^0 \right) \end{pmatrix}, \qquad \Phi = \begin{pmatrix} H^+ \\ \frac{1}{\sqrt{2}} \left(H^0 + \mathrm{i} A^0 \right) \end{pmatrix}. \quad (3.3)$$

The h^0 state corresponds to the physical SM-like Higgs-boson. The inert sector consists of a neutral CP-even scalar H^0, a pseudo-scalar A^0, and a pair of charged scalars $H^\pm$. The

$\mathbb{Z}_2$ symmetry guarantees the stability of the lightest state of the dark sector. If it is neutral (either H^0 or A^0), this state can play the role of the DM.

At the tree level, the scalar masses are

$$m_{h^0}^2 = \mu_1^2 + 3\lambda_1\, v_H^2\,, \tag{3.4}$$

$$m_{H^0}^2 = \mu_2^2 + \lambda_L\, v_H^2\,, \tag{3.5}$$

$$m_{A^0}^2 = \mu_2^2 + \lambda_S\, v_H^2\,, \tag{3.6}$$

$$m_{H^\pm}^2 = \mu_2^2 + \frac{1}{2}\lambda_3\, v_H^2\,, \tag{3.7}$$

where $\lambda_L \equiv \frac{1}{2}\left(\lambda_3 + \lambda_4 + \lambda_5\right)$ and $\lambda_S \equiv \frac{1}{2}\left(\lambda_3 + \lambda_4 - \lambda_5\right)$. The IDM scalar sector can be fully specified by a total of five parameters: three masses (m_{H^0}, m_{A^0} and $m_{H^\pm}$) and two couplings (λ_L and λ_2). However, in this analysis the role of λ_2 will be disregarded, as it appears only in quartic self couplings among dark particles and does therefore not enter in any physically observable process at the tree level.[8]

The phenomenology of the IDM has been largely studied since the model allows to generate a population of WIMP DM particles in the early Universe via a thermal freeze-out and it induces potentially observable signals in direct and indirect DM searches [75, 80, 80–92], collider searches [75, 79, 93–99] and electroweak precision tests [75, 100].

For this analysis, we perform a numerical analysis scanning randomly over $10\,\mathrm{GeV} < m_{H^0} < 1\,\mathrm{TeV}$, $10^{-5} < |\lambda_L| < 10^0$ and over m_{A^0} and $m_{H^\pm}$ in the range $[m_{H^0}, 10\,\mathrm{TeV}]$. A number of theoretical and experimental constraints, largely discussed in the literature, can be imposed on the parameters of the model like perturbativity, vacuum stability [89, 101, 102], unitarity of the S-matrix [103, 104], electroweak precision tests [97] and collider searches from LEP [94, 105] and LHC [79, 97–99, 105]. We restrict ourselves to the points fulfilling the observed DM relic abundance and the previously mentioned direct and indirect detection constraints.

Figure 7 shows the current constraints on the IDM plane ($|\lambda_L|$, m_{H^0}). In both panels, the visible dots correspond to those points of the parameter space that generates a DM relic abundance in agreement with Planck [72]. The light gray points in the upper left corner, however, are ruled out because they give rise to a too large invisible Higgs decay, in tension with LHC measurements [73, 74]. The left panel also displays the exclusion limit on the spin-independent elastic WIMP-nucleon cross section at 90% CL from the 2015 LUX results [37] for the choice of parameters in the first row of table 1 — as described in section 2.2, and shown as the red curve in figure 3 — which is translated into the dark red region in the top part of the figure. In the right panel, we show instead the points (light brown) in tension with the analysis of dSphs with *Fermi*-LAT [48]: the region in blue represents the parameter space favoured by the interpretation of the GC excess (at 2σ), and corresponds to the red contour in figure 5, as described in section 2.3. Let us emphasize that, as seen in figure 5, in this reference model the GC excess is in tension with the measurements of dSphs. Let us also point out that while the DM self-annihilation cross section (relevant for indirect detection and for the DM relic abundance) depends on basically all the parameters, the elastic scattering cross section for direct detection is controlled only by the DM mass and the λ_L coupling because it occurs via the t-channel exchange of a Higgs boson.

In figure 7 we study the constraints on the IDM parameter space coming from a specific Galactic model (i.e. the reference morphology model *BjX*). In section 4 we show the response

---

[8]Loop corrections to the WIMP DM phenomenology in the IDM have been studied in ref. [79].
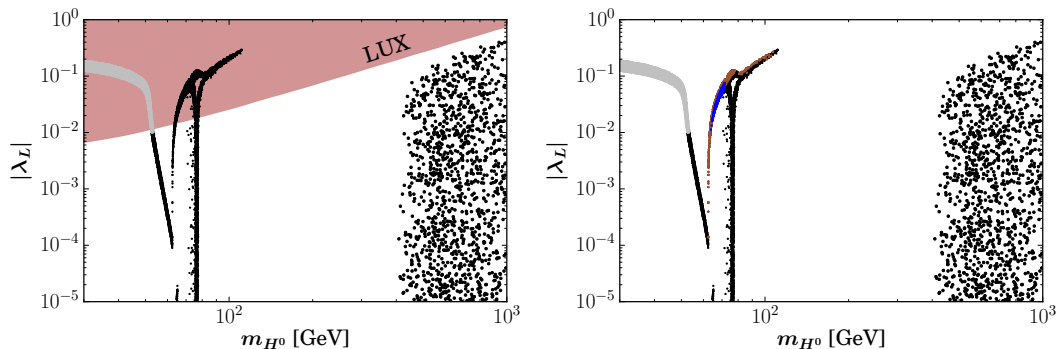
Figure 7. *Inert Doublet Model.* The dots correspond to the parameter space that generates the correct DM relic abundance. The light gray points give rise to a too large invisible Higgs decay, in tension with LHC measurements. The dark red region in the left panel displays the LUX exclusion limit on the spin-independent elastic WIMP-nucleon cross section at 90% CL for the choice of parameters in the first row of table 1. In the right panel, we show, in blue, the points of the parameter space which can successfully explain the GeV excess (at 2σ), corresponding to the red contour in figure 5. The points in light brown are those in tension with the analysis of dSphs with *Fermi*-LAT [48].

of the constraints to astrophysical uncertainties, and its implications for both direct and indirect DM searches.

4 Results

With all elements at hand, we now turn to show the effect of astrophysical uncertainties directly onto the parameter space of particle physics models discussed in the previous section.

4.1 Impact on SSDM parameter determination

We start by comparing the limit imposed by direct detection on the SSDM for different cases of variation of astrophysical uncertainties: in figure 8 we show how the LUX exclusion limit shown in the left panel of figure 6 varies by including uncertainties arising from *a)* the statistical uncertainty on our reference morphology, *b)* the variation of the Galactic parameters for the reference morphology, and *c)* the baryonic morphologies that maximize/minimize the local DM density ρ_0, as discussed in section 2.1.

As it can be seen, the statistical uncertainty related to the determination of the local DM density ρ_0 affects the determination of model parameters very little, thus justifying the fact that most of the literature neglects it. On the other hand, the uncertainty arising by either the ignorance about the exact value of Galactic parameters or the morphology of the visible component has sizable effects in shifting the constrained region in the parameter space. Notice that the largest uncertainty on the exclusion limit arises from the variation of the Galactic parameters. The reason is that this variation leads to a large variation in the value of ρ_0 (see the second and third rows of table 1) which is larger than the variation in ρ_0 due to either statistical uncertainties or the choice of morphology, with the latter still being quite sizable, as we will discuss in the following.

The situation is different if one looks at the GeV excess favored region versus the constraint imposed by dSphs. In figure 9, we show the effect of Galactic uncertainties on the GeV excess favored region in the SSDM parameter space. Blobs of different color shading
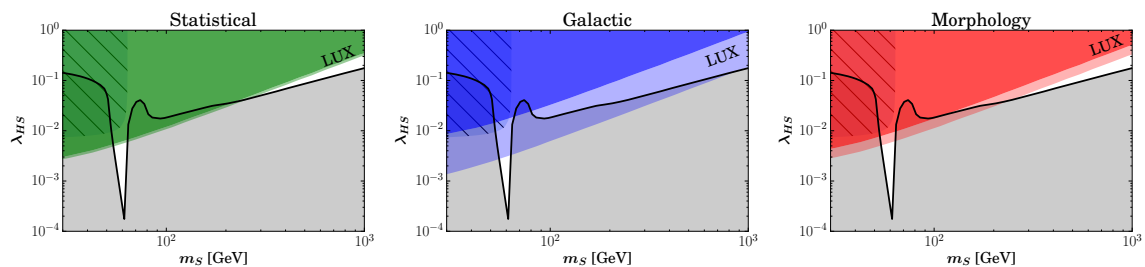
Figure 8. *Singlet Scalar Model*: effects of Galactic uncertainties on the LUX exclusion limit in the SSDM parameter space. We display the effect of: statistical uncertainty, for our reference morphology BjX (left panel); varying the Galactic parameters for the same reference morphology (central panel); adopting different morphologies that maximize/minimize the local DM density ρ_0, CjX and FiX (right panel). Criteria are discussed in section 2.1 and values are reported in table 1.
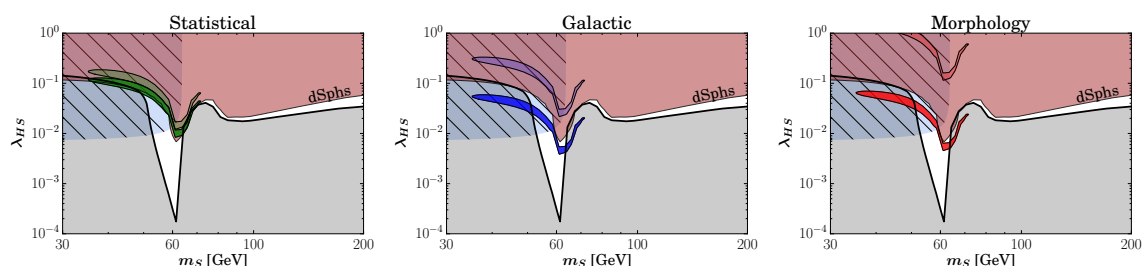
Figure 9. *Singlet Scalar Model*: effects of Galactic uncertainties following the GeV excess interpretation. We display the effect of: statistical uncertainty, for our reference morphology BjX left panel); changing the Galactic parameters, for the same reference morphology (central panel); adopting different morphologies that maximize/minimize the index γ, FkX and DiX (right panel). Criteria are discussed in section 2.1 and values are reported in table 1.

are the regions that explain the GeV excess at 2σ confidence level, shown as a red contour in figure 5, moving as a consequence of statistical, Galactic parameters, or baryonic morphology uncertainty. In this figure, for the baryonic morphology uncertainty, we choose the morphologies which maximise/minimise γ. As it can be easily seen, again the statistical uncertainty on a single morphology plays little role, not affecting conclusions, but the adoption of different Galactic parameters and morphologies sizably shift the favored region, relieving (or worsening) tension with dSphs constraints, as it was already seen in figure 5. It is interesting to notice that although the variation of Galactic parameters produces the most sizable alteration of the index γ and of ρ_0 (for assigned morphology, see table 1), these effects are partially compensated in the computation of the $\mathcal{J}$-factor, and the largest variation of the latter is obtained as a consequence of varying morphologies (for assigned Galactic parameters).

4.2 Impact on IDM parameter determination

Following closely the procedure described in the previous section, now we compare the limit imposed by direct detection on the IDM parameter space for different cases of variation of astrophysical uncertainties: in figure 10 we show how the LUX limit shown in the left panel of figure 7 varies by including uncertainties arising from *a)* the statistical uncertainty on our reference morphology, *b)* the variation of the Galactic parameters for the reference morphol-
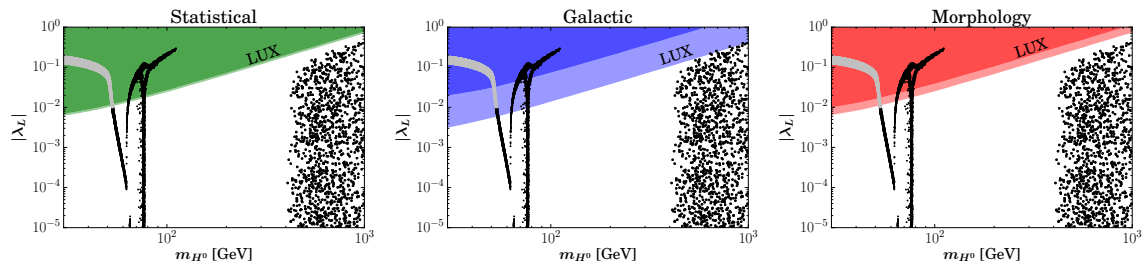
Figure 10. *Inert Doublet Model*: effects of Galactic uncertainties on the parameter constraints. We display the effect of: statistical uncertainty, for our reference morphology *BjX* left panel); changing Galactic parameters, for the same reference morphology (central panel); adopting different morphologies such as they maximize/minimize the local DM density ρ_0, *CjX* and *FiX* (right panel). Criteria are discussed in section 2.1 and values are reported in table 1.

ogy, and *c)* the baryonic morphologies that maximize/minimize the local DM density ρ_0, as discussed in section 2.1. For DM direct detection, the effects of the systematic uncertainties on the Galactic parameters on the IDM are similar to the ones on the SSDM: on one hand, the statistical uncertainty related to the determination of the local DM density ρ_0 affects mildly the determination of model parameters. On the other hand, the uncertainty arising by either the ignorance about the exact value of Galactic parameters or the morphology of the visible component has sizable effects in shifting the constrained region in the parameter space. As discussed before, the largest uncertainty in direct detection limits arises from the variation in the local DM density. The variation of the Galactic parameters for the reference morphology leads to the largest variation in ρ_0, and hence the largest uncertainty seen in the central panel of figure 10.

In figure 11, we show how the GC excess interpretation shown in the right panel of figure 7 varies with Galactic uncertainties. The dark gray dots show the constraint imposed by dSphs. Colored dots (green, blue and red) correspond to the regions of the parameter space that explain the GeV excess, moving as a consequence of statistical, Galactic, or morphology uncertainties, respectively. For the baryonic morphology uncertainty, we choose the morphologies which maximise/minimise γ. It can be seen from the figure that the regions that can simultaneously reproduce the measured DM relic abundance and explain the GC excess are quite reduced and typically in tension with the dSphs observations. Only marginal regions are allowed by the dSphs constraint when taking into account Galactic and morphological uncertainties.

It is to be noticed that figure 11 displays only one region of the parameter space, as favored by the GC excess interpretation for both the Galactic parameters and the morphology, differently than in the case of SSDM. The variation of both morphology and Galactic parameters impose a change in the IDM parameters (similar to what happens with the SSDM), but in both cases this shift ends up in a region which cannot reproduce the DM relic abundance. The "shifted" region is not visible in the figure as it is forbidden by the cosmological constraint, which henceforth practically sets limits on the DM interpretation of the GC excess, but only for some combinations of the Galactic parameters.
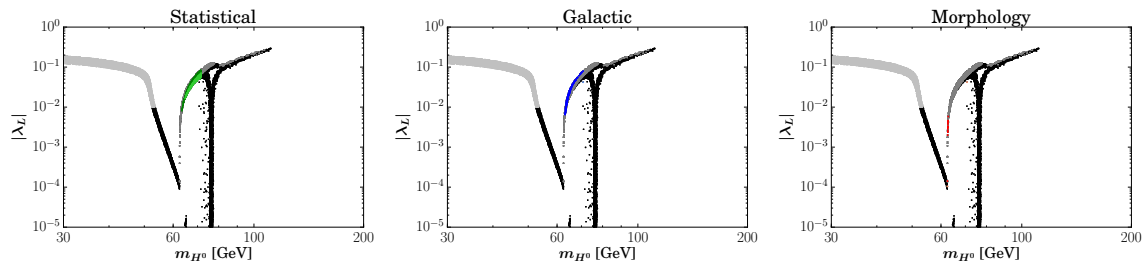
Figure 11. *Inert Doublet Model*: effects of Galactic uncertainties following the GC excess interpretation. We display the effect of: statistical uncertainty, for our reference morphology *BjX* (left panel); changing Galactic parameters, for the same reference morphology (central panel); adopting different morphologies such as they maximize/minimize the index γ, *FkX* and *DiX* (right panel). Criteria are discussed in section 2.1 and values are reported in table 1. The colored dots (green, blue and red) correspond to the regions of the parameter space that explain the GC GeV excess; the dark gray dots are in tension with the constraint imposed by dSphs.

5 Conclusions

In this work we have studied how the uncertainties associated to Galactic core quantities, such as the local galactocentric distance, local circular velocity, and the morphology of the stellar disk and bulge, affect the determination of DM distribution, and eventually propagate when constraining new physics scenarios. We have set up a systematic scan of the major sources of uncertainty in the determination of the DM distribution in the MW, testing (a) statistical uncertainties; (b) variation of Galactic parameters; (c) variation of baryonic morphology. While the purely statistical uncertainties affecting the observed RC and the normalization of the visible mass component do not sizably affect the constraints on new physics model parameters, a significant impact on the allowed model parameter space is due to the current ignorance on the morphology of the baryonic component, and on the determination of Galactic parameters.

We have shown that the latter significantly affect the constraints of two specific models, the SSDM and the IDM, which we have chosen as testbeds for the relatively simple dependence of their phenomenology on the key parameters. Our main findings, which we summarize below, show the need for the study of these uncertainties in more complex scenarios, and an increased communication between the particle physics and the astronomy communities in a virtuous interplay.

The largest effects on the SSDM and IDM parameter space are obtained as a consequence of varying the Galactic parameters (R_0, v_0): the variation of (R_0, v_0) between its currently established extreme values pushes the determination of the local DM density ρ_0 beyond the usually adopted bounds (which are taken for assigned Galactic parameters, and include statistical uncertainty only, in most cases), with major effects especially on direct detection results. Interestingly, the remarkable changes imposed by the Galactic parameter variation also on the index γ mitigate the effect on the determination of the $\mathcal{J}$-factor, which sees the uncertainty on the baryonic morphology as a primary source of uncertainty for indirect detection.

As an example of the above, we recall here the case of SSDM: the region of the parameter space which permits an interpretation of the GC excess in terms of DM annihilation is allowed with a given set of Galactic parameters, but it could be also entirely ruled out by constraints on the relic density if the other extreme values for (R_0, v_0) are adopted.

Accounting for the astrophysical uncertainties described above, will be even more crucial in the case a tantalising DM signal will be discovered in the next-generation of direct and indirect experiments. In that case, the accurate reconstruction and interpretation of the signal in the context of concrete particle physics models will require the full treatment of all astrophysical uncertainties presented in our work.

On the other hand, future astronomical data will help in reducing significantly those uncertainties. In particular, the *Gaia* mission is expected to improve the determination of the Oort constants, and yield a reduction of uncertainties on the determination of (R_0, v_0), as already shown possible with the first year data release [106].

Acknowledgments

References

[1] J.I. Read, *The Local Dark Matter Density*, *J. Phys.* **G 41** (2014) 063101 [`arXiv:1404.1938`] [INSPIRE].

[2] M. Pato, F. Iocco and G. Bertone, *Dynamical constraints on the dark matter distribution in the Milky Way*, *JCAP* **12** (2015) 001 [`arXiv:1504.06324`] [INSPIRE].

[3] R. Catena and P. Ullio, *A novel determination of the local dark matter density*, *JCAP* **08** (2010) 004 [`arXiv:0907.0018`] [INSPIRE].

[4] F. Iocco, M. Pato, G. Bertone and P. Jetzer, *Dark Matter distribution in the Milky Way: microlensing and dynamical constraints*, *JCAP* **11** (2011) 029 [`arXiv:1107.5810`] [INSPIRE].

[5] F. Nesti and P. Salucci, *The Dark Matter halo of the Milky Way, AD 2013*, *JCAP* **07** (2013) 016 [`arXiv:1304.5127`] [INSPIRE].

[6] F. Iocco, M. Pato and G. Bertone, *Evidence for dark matter in the inner Milky Way*, *Nature Phys.* **11** (2015) 245 [`arXiv:1502.03821`] [INSPIRE].

[7] N. Bozorgnia, F. Calore, M. Schaller, M. Lovell, G. Bertone, C.S. Frenk et al., *Simulated Milky Way analogues: implications for dark matter direct searches*, *JCAP* **05** (2016) 024 [`arXiv:1601.04707`] [INSPIRE].

[8] E. Dwek, R.G. Arendt, M.G. Hauser, T. Kelsall, C.M. Lisse, S.H. Moseley et al., *Morphology, near infrared luminosity and mass of the galactic bulge from Cobe dirbe observations*, *Astrophys. J.* **445** (1995) 716 [INSPIRE].

[9] C. Han and A.P. Gould, *Stellar contribution to the Galactic bulge microlensing optical depth*, *Astrophys. J.* **592** (2003) 172 [`astro-ph/0303309`] [INSPIRE].

[10] K. Ferriere, W. Gillard and P. Jean, *Spatial distribution of interstellar gas in the innermost 3 kpc of our Galaxy*, *Astron. Astrophys.* **467** (2007) 611 [`astro-ph/0702532`] [INSPIRE].

[11] K. Ferriere, *Global Model of the Interstellar Medium in Our Galaxy with New Constraints on the Hot Gas Component*, *Astrophys. J.* **497** (1998) 759.

[12] P.J. McMillan and J.J. Binney, *The uncertainty in Galactic parameters*, *Mon. Not. Roy. Astron. Soc.* **402** (2010) 934 [arXiv:0907.4685].

[13] M. Pato and F. Iocco, galkin: *A new compilation of the Milky Way rotation curve*, *SoftwareX* **6** (2017) 54.

[14] M.I. Wilkinson and N.W. Evans, *The present and future mass of the Milky Way halo*, *Mon. Not. Roy. Astron. Soc.* **310** (1999) 645 [astro-ph/9906197].

[15] T. Sakamoto, M. Chiba and T.C. Beers, *The Mass of the Milky Way: Limits from a newly assembled set of halo objects*, *Astron. Astrophys.* **397** (2003) 899 [astro-ph/0210508] [INSPIRE].

[16] M.C. Smith et al., *The RAVE Survey: constraining the Local Galactic Escape Speed*, *Mon. Not. Roy. Astron. Soc.* **379** (2007) 755 [astro-ph/0611671].

[17] A.J. Deason, V. Belokurov, N.W. Evans and J.H. An, *Broken Degeneracies: the Rotation Curve and Velocity Anisotropy of the Milky Way Halo*, *Mon. Not. Roy. Astron. Soc.* **424** (2012) L44 [arXiv:1204.5189].

[18] S.L.J. Gibbons, V. Belokurov and N.W. Evans, *'Skinny Milky Way please', says Sagittarius*, *Mon. Not. Roy. Astron. Soc.* **445** (2014) 3788 [arXiv:1406.2243] [INSPIRE].

[19] G. Besla, N. Kallivayalil, L. Hernquist, B. Robertson, T.J. Cox, R.P. van der Marel et al., *Are the Magellanic Clouds on their First Passage about the Milky Way?*, *Astrophys. J.* **668** (2007) 949 [astro-ph/0703196] [INSPIRE].

[20] M. Portail, C. Wegg, O. Gerhard and I. Martinez-Valpuesta, *Made-to-measure models of the galactic box/peanut bulge: stellar and total mass in the bulge region*, *Mon. Not. Roy. Astron. Soc.* **448** (2015) 713 [arXiv:1502.00633].

[21] F. Iocco and M. Benito, *An estimate of the DM profile in the Galactic bulge region*, *Phys. Dark Univ.* **15** (2017) 90 [arXiv:1611.09861] [INSPIRE].

[22] F. Calore, N. Bozorgnia, M. Lovell, G. Bertone, M. Schaller, C.S. Frenk et al., *Simulated Milky Way analogues: implications for dark matter indirect searches*, *JCAP* **12** (2015) 053 [arXiv:1509.02164] [INSPIRE].

[23] M. Schaller et al., *Dark matter annihilation radiation in hydrodynamic simulations of Milky Way haloes*, *Mon. Not. Roy. Astron. Soc.* **455** (2016) 4442 [arXiv:1509.02166] [INSPIRE].

[24] A.C. Robin, D.J. Marshall, M. Schultheis and C. Reyle, *Stellar populations in the Milky Way bulge region : Towards solving the Galactic bulge and bar shapes using 2MASS data*, *Astron. Astrophys.* **538** (2012) A106 [arXiv:1111.5744] [INSPIRE].

[25] S. Calchi Novati and L. Mancini, *Microlensing towards the LMC: self lensing for OGLE-II and OGLE-III*, *Mon. Not. Roy. Astron. Soc.* **416** (2011) 1292 [arXiv:1105.4615].

[26] N. Bissantz and O. Gerhard, *Spiral arms, bar shape and bulge microlensing in the milky way*, *Mon. Not. Roy. Astron. Soc.* **330** (2002) 591 [astro-ph/0110368].

[27] J. Bovy and H.-W. Rix, *A Direct Dynamical Measurement of the Milky Way's Disk Surface Density Profile, Disk Scale Length and Dark Matter Profile at 4 kpc $\lesssim$ R $\lesssim$ 9 kpc*, *Astrophys. J.* **779** (2013) 115 [arXiv:1309.0809] [INSPIRE].

[28] E. Vanhollebeke, M.A.T. Groenewegen and L. Girardi, *Stellar populations in the Galactic bulge*, arXiv:0903.0946 [INSPIRE].

[29] R. Bernabei et al., *Final model independent result of DAMA/LIBRA-phase1*, *Eur. Phys. J.* **C 73** (2013) 2648 [arXiv:1308.5109] [INSPIRE].

[30] CDMS collaboration, R. Agnese et al., *Silicon Detector Dark Matter Results from the Final Exposure of CDMS II*, *Phys. Rev. Lett.* **111** (2013) 251301 [arXiv:1304.4279] [INSPIRE].

[31] CoGeNT collaboration, C.E. Aalseth et al., *Results from a Search for Light-Mass Dark Matter with a P-type Point Contact Germanium Detector*, *Phys. Rev. Lett.* **106** (2011) 131301 [arXiv:1002.4703] [INSPIRE].

[32] CoGeNT collaboration, C.E. Aalseth et al., *Search for An Annual Modulation in Three Years of CoGeNT Dark Matter Detector Data*, arXiv:1401.3295 [INSPIRE].

[33] LUX collaboration, D.S. Akerib et al., *Results from a search for dark matter in the complete LUX exposure*, *Phys. Rev. Lett.* **118** (2017) 021303 [arXiv:1608.07648] [INSPIRE].

[34] PandaX-II collaboration, A. Tan et al., *Dark Matter Results from First 98.7 Days of Data from the PandaX-II Experiment*, *Phys. Rev. Lett.* **117** (2016) 121303 [arXiv:1607.07400] [INSPIRE].

[35] R. Schönrich, J. Binney and W. Dehnen, *Local Kinematics and the Local Standard of Rest*, *Mon. Not. Roy. Astron. Soc.* **403** (2010) 1829 [arXiv:0912.3693].

[36] T. Piffl et al., *The RAVE survey: the Galactic escape speed and the mass of the Milky Way*, *Astron. Astrophys.* **562** (2014) A91 [arXiv:1309.4293] [INSPIRE].

[37] LUX collaboration, D.S. Akerib et al., *Improved Limits on Scattering of Weakly Interacting Massive Particles from Reanalysis of 2013 LUX Data*, *Phys. Rev. Lett.* **116** (2016) 161301 [arXiv:1512.03506] [INSPIRE].

[38] S. Yellin, *Finding an upper limit in the presence of unknown background*, *Phys. Rev.* **D 66** (2002) 032005 [physics/0203002] [INSPIRE].

[39] F. Calore, I. Cholis and C. Weniger, *Background Model Systematics for the Fermi GeV Excess*, *JCAP* **03** (2015) 038 [arXiv:1409.0042] [INSPIRE].

[40] Fermi-LAT collaboration, M. Ajello et al., *Fermi-LAT Observations of High-Energy γ-Ray Emission Toward the Galactic Center*, *Astrophys. J.* **819** (2016) 44 [arXiv:1511.02938] [INSPIRE].

[41] I. Cholis, D. Hooper and T. Linden, *Challenges in Explaining the Galactic Center Gamma-Ray Excess with Millisecond Pulsars*, *JCAP* **06** (2015) 043 [arXiv:1407.5625] [INSPIRE].

[42] J. Petrović, P.D. Serpico and G. Zaharijas, *Millisecond pulsars and the Galactic Center gamma-ray excess: the importance of luminosity function and secondary emission*, *JCAP* **02** (2015) 023 [arXiv:1411.2980] [INSPIRE].

[43] J. Petrović, P.D. Serpico and G. Zaharijaš, *Galactic Center gamma-ray "excess" from an active past of the Galactic Centre?*, *JCAP* **10** (2014) 052 [arXiv:1405.7928] [INSPIRE].

[44] F. Calore, M. Di Mauro, F. Donato and F. Donato, *Diffuse gamma-ray emission from galactic pulsars*, *Astrophys. J.* **796** (2014) 1 [arXiv:1406.2706] [INSPIRE].

[45] I. Cholis, C. Evoli, F. Calore, T. Linden, C. Weniger and D. Hooper, *The Galactic Center GeV Excess from a Series of Leptonic Cosmic-Ray Outbursts*, *JCAP* **12** (2015) 005 [arXiv:1506.05119] [INSPIRE].

[46] F. Calore, I. Cholis, C. McCabe and C. Weniger, *A Tale of Tails: Dark Matter Interpretations of the Fermi GeV Excess in Light of Background Model Systematics*, *Phys. Rev.* **D 91** (2015) 063003 [arXiv:1411.4647] [INSPIRE].

[47] G. Bertone, F. Calore, S. Caron, R. Ruiz, J.S. Kim, R. Trotta et al., *Global analysis of the pMSSM in light of the Fermi GeV excess: prospects for the LHC Run-II and astroparticle experiments*, *JCAP* **04** (2016) 037 [arXiv:1507.07008] [INSPIRE].

[48] DES and FERMI-LAT collaborations, A. Albert et al., *Searching for Dark Matter Annihilation in Recently Discovered Milky Way Satellites with Fermi-LAT*, *Astrophys. J.* **834** (2017) 110 [arXiv:1611.03184] [INSPIRE].

[49] L.E. Strigari, *Galactic Searches for Dark Matter*, *Phys. Rept.* **531** (2013) 1 [arXiv:1211.7090] [INSPIRE].

[50] DES collaboration, A. Drlica-Wagner et al., *Eight Ultra-faint Galaxy Candidates Discovered in Year Two of the Dark Energy Survey*, *Astrophys. J.* **813** (2015) 109 [arXiv:1508.03622] [INSPIRE].

[51] J. McDonald, *Gauge singlet scalars as cold dark matter*, *Phys. Rev.* **D 50** (1994) 3637 [hep-ph/0702143] [INSPIRE].

[52] C.P. Burgess, M. Pospelov and T. ter Veldhuis, *The Minimal model of nonbaryonic dark matter: A Singlet scalar*, *Nucl. Phys.* **B 619** (2001) 709 [hep-ph/0011335] [INSPIRE].

[53] N. Bernal and X. Chu, Z_2 *SIMP Dark Matter*, *JCAP* **01** (2016) 006 [arXiv:1510.08527] [INSPIRE].

[54] V. Barger, P. Langacker, M. McCaskey, M.J. Ramsey-Musolf and G. Shaughnessy, *LHC Phenomenology of an Extended Standard Model with a Real Scalar Singlet*, *Phys. Rev.* **D 77** (2008) 035005 [arXiv:0706.4311] [INSPIRE].

[55] A. Djouadi, O. Lebedev, Y. Mambrini and J. Quevillon, *Implications of LHC searches for Higgs–portal dark matter*, *Phys. Lett.* **B 709** (2012) 65 [arXiv:1112.3299] [INSPIRE].

[56] A. Djouadi, A. Falkowski, Y. Mambrini and J. Quevillon, *Direct Detection of Higgs-Portal Dark Matter at the LHC*, *Eur. Phys. J.* **C 73** (2013) 2455 [arXiv:1205.3169] [INSPIRE].

[57] P.H. Damgaard, D. O'Connell, T.C. Petersen and A. Tranberg, *Constraints on New Physics from Baryogenesis and Large Hadron Collider Data*, *Phys. Rev. Lett.* **111** (2013) 221804 [arXiv:1305.4362] [INSPIRE].

[58] J.M. No and M. Ramsey-Musolf, *Probing the Higgs Portal at the LHC Through Resonant di-Higgs Production*, *Phys. Rev.* **D 89** (2014) 095031 [arXiv:1310.6035] [INSPIRE].

[59] T. Robens and T. Stefaniak, *Status of the Higgs Singlet Extension of the Standard Model after LHC Run 1*, *Eur. Phys. J.* **C 75** (2015) 104 [arXiv:1501.02234] [INSPIRE].

[60] H. Han, J.M. Yang, Y. Zhang and S. Zheng, *Collider Signatures of Higgs-portal Scalar Dark Matter*, *Phys. Lett.* **B 756** (2016) 109 [arXiv:1601.06232] [INSPIRE].

[61] X.-G. He, T. Li, X.-Q. Li, J. Tandean and H.-C. Tsai, *The Simplest Dark-Matter Model, CDMS II Results and Higgs Detection at LHC*, *Phys. Lett.* **B 688** (2010) 332 [arXiv:0912.4722] [INSPIRE].

[62] S. Baek, P. Ko and W.-I. Park, *Invisible Higgs Decay Width vs. Dark Matter Direct Detection Cross Section in Higgs Portal Dark Matter Models*, *Phys. Rev.* **D 90** (2014) 055014 [arXiv:1405.3530] [INSPIRE].

[63] L. Feng, S. Profumo and L. Ubaldi, *Closing in on singlet scalar dark matter: LUX, invisible Higgs decays and gamma-ray lines*, *JHEP* **03** (2015) 045 [arXiv:1412.1105] [INSPIRE].

[64] H. Han and S. Zheng, *New Constraints on Higgs-portal Scalar Dark Matter*, *JHEP* **12** (2015) 044 [arXiv:1509.01765] [INSPIRE].

[65] C.E. Yaguna, *Gamma rays from the annihilation of singlet scalar dark matter*, *JCAP* **03** (2009) 003 [arXiv:0810.4267] [INSPIRE].

[66] A. Goudelis, Y. Mambrini and C. Yaguna, *Antimatter signals of singlet scalar dark matter*, *JCAP* **12** (2009) 008 [arXiv:0909.2799] [INSPIRE].

[67] S. Profumo, L. Ubaldi and C. Wainwright, *Singlet Scalar Dark Matter: monochromatic gamma rays and metastable vacua*, *Phys. Rev.* **D 82** (2010) 123514 [arXiv:1009.5377] [INSPIRE].

[68] J.M. Cline, K. Kainulainen, P. Scott and C. Weniger, *Update on scalar singlet dark matter*, *Phys. Rev.* **D 88** (2013) 055025 [arXiv:1306.4710] [INSPIRE].

[69] A. Urbano and W. Xue, *Constraining the Higgs portal with antiprotons*, *JHEP* **03** (2015) 133 [arXiv:1412.3798] [INSPIRE].

[70] M. Duerr, P. Fileviez Perez and J. Smirnov, *Scalar Singlet Dark Matter and Gamma Lines*, *Phys. Lett.* **B 751** (2015) 119 [arXiv:1508.04418] [INSPIRE].

[71] M. Duerr, P. Fileviez Pérez and J. Smirnov, *Scalar Dark Matter: Direct vs. Indirect Detection*, *JHEP* **06** (2016) 152 [arXiv:1509.04282] [INSPIRE].

[72] PLANCK collaboration, P.A.R. Ade et al., *Planck 2015 results. XIII. Cosmological parameters*, *Astron. Astrophys.* **594** (2016) A13 [arXiv:1502.01589] [INSPIRE].

[73] P. Bechtle, S. Heinemeyer, O. Stål, T. Stefaniak and G. Weiglein, *Probing the Standard Model with Higgs signal rates from the Tevatron, the LHC and a future ILC*, *JHEP* **11** (2014) 039 [arXiv:1403.1582] [INSPIRE].

[74] CMS collaboration, *Constraints on the Higgs boson width from off-shell production and decay to Z-boson pairs*, *Phys. Lett.* **B 736** (2014) 64 [arXiv:1405.3455] [INSPIRE].

[75] R. Barbieri, L.J. Hall and V.S. Rychkov, *Improved naturalness with a heavy Higgs: An Alternative road to LHC physics*, *Phys. Rev.* **D 74** (2006) 015007 [hep-ph/0603188] [INSPIRE].

[76] T.A. Chowdhury, M. Nemevšek, G. Senjanović and Y. Zhang, *Dark Matter as the Trigger of Strong Electroweak Phase Transition*, *JCAP* **02** (2012) 029 [arXiv:1110.5334] [INSPIRE].

[77] D. Borah and J.M. Cline, *Inert Doublet Dark Matter with Strong Electroweak Phase Transition*, *Phys. Rev.* **D 86** (2012) 055001 [arXiv:1204.4722] [INSPIRE].

[78] J.M. Cline and K. Kainulainen, *Improved Electroweak Phase Transition with Subdominant Inert Doublet Dark Matter*, *Phys. Rev.* **D 87** (2013) 071701 [arXiv:1302.2614] [INSPIRE].

[79] A. Goudelis, B. Herrmann and O. Stål, *Dark matter in the Inert Doublet Model after the discovery of a Higgs-like boson at the LHC*, *JHEP* **09** (2013) 106 [arXiv:1303.3010] [INSPIRE].

[80] D. Majumdar and A. Ghosal, *Dark Matter candidate in a Heavy Higgs Model - Direct Detection Rates*, *Mod. Phys. Lett.* **A 23** (2008) 2011 [hep-ph/0607067] [INSPIRE].

[81] L. Lopez Honorez, E. Nezri, J.F. Oliver and M.H.G. Tytgat, *The Inert Doublet Model: An Archetype for Dark Matter*, *JCAP* **02** (2007) 028 [hep-ph/0612275] [INSPIRE].

[82] M. Gustafsson, E. Lundström, L. Bergström and J. Edsjö, *Significant Gamma Lines from Inert Higgs Dark Matter*, *Phys. Rev. Lett.* **99** (2007) 041301 [astro-ph/0703512] [INSPIRE].

[83] P. Agrawal, E.M. Dolle and C.A. Krenke, *Signals of Inert Doublet Dark Matter in Neutrino Telescopes*, *Phys. Rev.* **D 79** (2009) 015015 [arXiv:0811.1798] [INSPIRE].

[84] S. Andreas, M.H.G. Tytgat and Q. Swillens, *Neutrinos from Inert Doublet Dark Matter*, *JCAP* **04** (2009) 004 [arXiv:0901.1750] [INSPIRE].

[85] E. Nezri, M.H.G. Tytgat and G. Vertongen, *e+ and p̄ from inert doublet model dark matter*, *JCAP* **04** (2009) 014 [arXiv:0901.2556] [INSPIRE].

[86] C. Arina, F.-S. Ling and M.H.G. Tytgat, *IDM and iDM or The Inert Doublet Model and Inelastic Dark Matter*, *JCAP* **10** (2009) 018 [arXiv:0907.0430] [INSPIRE].

[87] L. Lopez Honorez and C.E. Yaguna, *The inert doublet model of dark matter revisited*, *JHEP* **09** (2010) 046 [arXiv:1003.3125] [INSPIRE].

[88] L. Lopez Honorez and C.E. Yaguna, *A new viable region of the inert doublet model*, *JCAP* **01** (2011) 002 [arXiv:1011.1411] [INSPIRE].

[89] M. Gustafsson, *The Inert Doublet Model and Its Phenomenology*, PoS(Charged 2010)030 [arXiv:1106.1719] [INSPIRE].

[90] M. Klasen, C.E. Yaguna and J.D. Ruiz-Alvarez, *Electroweak corrections to the direct detection cross section of inert Higgs dark matter*, *Phys. Rev.* **D 87** (2013) 075025 [arXiv:1302.1657] [INSPIRE].

[91] C. Garcia-Cely and A. Ibarra, *Novel Gamma-ray Spectral Features in the Inert Doublet Model*, *JCAP* **09** (2013) 025 [arXiv:1306.4681] [INSPIRE].

[92] C. Garcia-Cely, M. Gustafsson and A. Ibarra, *Probing the Inert Doublet Dark Matter Model with Cherenkov Telescopes*, *JCAP* **02** (2016) 043 [arXiv:1512.02801] [INSPIRE].

[93] Q.-H. Cao, E. Ma and G. Rajasekaran, *Observing the Dark Scalar Doublet and its Impact on the Standard-Model Higgs Boson at Colliders*, *Phys. Rev.* **D 76** (2007) 095011 [arXiv:0708.2939] [INSPIRE].

[94] E. Lundstrom, M. Gustafsson and J. Edsjo, *The Inert Doublet Model and LEP II Limits*, *Phys. Rev.* **D 79** (2009) 035013 [arXiv:0810.3924] [INSPIRE].

[95] E. Dolle, X. Miao, S. Su and B. Thomas, *Dilepton Signals in the Inert Doublet Model*, *Phys. Rev.* **D 81** (2010) 035003 [arXiv:0909.3094] [INSPIRE].

[96] X. Miao, S. Su and B. Thomas, *Trilepton Signals in the Inert Doublet Model*, *Phys. Rev.* **D 82** (2010) 035009 [arXiv:1005.0090] [INSPIRE].

[97] A. Arhrib, R. Benbrik and N. Gaur, *H → γγ in Inert Higgs Doublet Model*, *Phys. Rev.* **D 85** (2012) 095021 [arXiv:1201.2644] [INSPIRE].

[98] B. Świeżewska and M. Krawczyk, *Diphoton rate in the inert doublet model with a 125 GeV Higgs boson*, *Phys. Rev.* **D 88** (2013) 035019 [arXiv:1212.4100] [INSPIRE].

[99] M. Krawczyk, D. Sokolowska, P. Swaczyna and B. Świeżewska, *Constraining Inert Dark Matter by $R_{\gamma\gamma}$ and WMAP data*, *JHEP* **09** (2013) 055 [arXiv:1305.6266] [INSPIRE].

[100] W. Grimus, L. Lavoura, O.M. Ogreid and P. Osland, *The Oblique parameters in multi-Higgs-doublet models*, *Nucl. Phys.* **B 801** (2008) 81 [arXiv:0802.4353] [INSPIRE].

[101] J.F. Gunion and H.E. Haber, *The CP conserving two Higgs doublet model: The Approach to the decoupling limit*, *Phys. Rev.* **D 67** (2003) 075019 [hep-ph/0207010] [INSPIRE].

[102] N. Khan and S. Rakshit, *Constraints on inert dark matter from the metastability of the electroweak vacuum*, *Phys. Rev.* **D 92** (2015) 055006 [arXiv:1503.03085] [INSPIRE].

[103] I.F. Ginzburg and M. Krawczyk, *Symmetries of two Higgs doublet model and CP-violation*, *Phys. Rev.* **D 72** (2005) 115013 [hep-ph/0408011] [INSPIRE].

[104] G.C. Branco, P.M. Ferreira, L. Lavoura, M.N. Rebelo, M. Sher and J.P. Silva, *Theory and phenomenology of two-Higgs-doublet models*, *Phys. Rept.* **516** (2012) 1 [arXiv:1106.0034] [INSPIRE].

[105] A. Pierce and J. Thaler, *Natural Dark Matter from an Unnatural Higgs Boson and New Colored Particles at the TeV Scale*, *JHEP* **08** (2007) 026 [hep-ph/0703056] [INSPIRE].

[106] J. Bovy, *Galactic rotation in Gaia DR1*, arXiv:1610.07610.